ORIGINAL ARTICLE

Cancer Science WILEY

Patient-derived xenograft models of non-small cell lung cancer for evaluating targeted drug sensitivity and resistance

Kenji Kita[1,2] | Koji Fukuda[1,3] | Hiro Takahashi[4] | Azusa Tanimoto[1] | Akihiro Nishiyama[1] | Sachiko Arai[1,2] | Shinji Takeuchi[1,3] | Kaname Yamashita[1] | Koshiro Ohtsubo[1] | Sakiko Otani[1] | Naohiro Yanagimura[1] | Chiaki Suzuki[1] | Hiroko Ikeda[5] | Masaya Tamura[6] | Isao Matsumoto[6] | Seiji Yano[1,3]

[1]Division of Medical Oncology, Cancer Research Institute, Kanazawa University, Kanazawa, Japan

[2]Central Research Resource Branch, Cancer Research Institute, Kanazawa University, Kanazawa, Japan

[3]Nano Life Science Institute, Kanazawa University, Kanazawa, Japan

[4]Graduate School of Medical Sciences, Kanazawa University, Kanazawa, Japan

[5]Division of Pathology, Kanazawa University Hospital, Kanazawa, Japan

[6]Department of Thoracic, Cardiovascular and General Surgery, Kanazawa University, Kanazawa, Japan

Correspondence
Seiji Yano, Division of Medical Oncology, Cancer Research Institute Kanazawa University, Kanazawa, Japan.
Email: syano@staff.kanazawa-u.ac.jp

Abstract

Patient-derived xenograft (PDX) models are a useful tool in cancer biology research. However, the number of lung cancer PDX is limited. In the present study, we successfully established 10 PDX, including three adenocarcinoma (AD), six squamous cell carcinoma (SQ) and one large cell carcinoma (LA), from 30 patients with non-small cell lung cancer (NSCLC) (18 AD, 10 SQ, and 2 LA), mainly in SCID hairless outbred (SHO) mice (Crlj:SHO-Prkdc^{scid}Hr^{hr}). Histology of SQ, advanced clinical stage (III-IV), status of lymph node metastasis (N2-3), and maximum standardized uptake value ≥10 when evaluated using a delayed ^{18}F-fluoro-2-deoxy-D-glucose positron emission tomography (FDG-PET) scan was associated with successful PDX establishment. Histological analyses showed that PDX had histology similar to that of patients' surgically resected tumors (SRT), whereas components of the microenvironment were replaced with murine cells after several passages. Next-generation sequencing analyses showed that after two to six passages, PDX preserved the majority of the somatic mutations and mRNA expressions of the corresponding SRT. Two out of three PDX with AD histology had epidermal growth factor receptor (*EGFR*) mutations (L858R or exon 19 deletion) and were sensitive to EGFR tyrosine kinase inhibitors (EGFR-TKI), such as gefitinib and osimertinib. Furthermore, in one of the two PDX with an *EGFR* mutation, osimertinib resistance was induced that was associated with epithelial-to-mesenchymal transition. This study presented 10 serially transplantable PDX of NSCLC in SHO mice and showed the use of PDX with an *EGFR* mutation for analyses of EGFR-TKI resistance.

KEYWORDS
EGFR mutation, EGFR-TKI, non-small cell lung cancer, patient-derived xenograft, SHO mouse

---

1 | INTRODUCTION

Patient-derived xenograft models are considered superior to cell line-derived xenograft (CDX) models in preserving characteristics of patient tumors, and are thus more suitable for use in experiments exploring the molecular mechanisms of tumor progression and drug resistance.[1] Many studies have reported the establishment of various types of cancer models.[2-6] Among them, lung cancer is the leading cause of cancer death worldwide. Novel therapeutic approaches are needed to improve the poor prognoses for patients with this disease. Although the number of lung cancer PDX is gradually increasing, more are necessary for a better understanding of the mechanisms by which lung cancer progresses and develops resistance to certain drugs. Optimal methods for the establishment of lung cancer PDX, including the strain of recipient mice, need to be determined.

Several types of immunodeficient mice are used as recipients for the establishment of lung cancer PDX with varying success.[2-8] These include athymic nude, SCID, and non-obese diabetic (NOD)-SCID mice. In the present study, we attempted to establish PDX using 30 SRT from NSCLC patients. We compared somatic gene mutations, copy number, and mRNA expression in SRT with the corresponding PDX. Additionally, we examined the sensitivity of PDX with EGFR mutations to EGFR-TKI and induced acquired resistance to EGFR-TKI using the PDX model.

2 | MATERIALS AND METHODS

2.1 | Patients and PDX establishment

All pdx experiments in this paper were approved by the Institutional Review Board of Kanazawa University. Patient tumor samples were obtained with informed consent. Tumor specimens were divided into small pieces (3-5 mm) and implanted into the subcutaneous flank tissue of female NOD-SCID gamma mice (NOD.Cg-Prkdc^{scid}Il2rg^{tm1Sug}/ShiJic; Central Institute for Experimental Animals) and female SHO mice (Crlj:SHO-Prkdc^{scid}Hr^{hr}, Charles River). Tumor size was measured with calipers once a week. When tumors reached 1.0-1.5 cm in diameter, mice were killed and tumors were implanted into new mice and passaged a minimum of three times to establish model stability.

2.2 | Histological analyses

Surgically resected tumors and PDX were formalin fixed and embedded in paraffin. H&E staining was used for assessment of pathology. For immunohistochemistry (IHC), 5-μm thick sections were treated with primary antibodies against human PD-L1 (22C3; Dako), human MHC class I (Hokudo), human CD8 (Dako), human CD31 (Leica), human CD68 (Dako), human myeloperoxidase, α-smooth muscle actin (α-SMA; Thermo Fisher Scientific), mouse CD31 (Abcam), and mouse F4 80 (Cedarlane). Next, they were incubated with secondary antibodies at room temperature and treated with Vectastain ABC Kit (Vector Laboratories). 3,3′-Diaminobenzidine reaction was visualized by peroxidase activity.

2.3 | Library preparation and sequencing for whole-exome sequencing

DNA from PDX and SRT was extracted using Gen Elute Mammalian Genomic DNA Miniprep kits (Sigma-Aldrich). Each total genome sample (1.2 μg), extracted from six paired samples of PDX and SRT, was used for whole-exome sequencing (WES) library constructed using SureSelect Human All Exon V6 (Agilent Technologies), according to the manufacturer protocols. These samples were sheared into approximately 200-bp fragments, and used to make a library for multiplexed paired-end sequencing with the SureSelect Reagent Kit (Agilent Technologies). After fragmentation, captured libraries included inserts ranging in peak size from 311 bp to 335 bp. The constructed library was hybridized with biotinylated cRNA oligonucleotide baits from the SureSelect Human All Exon V6 Kit (Agilent Technologies) for target enrichment. Targeted sequence libraries were purified by magnetic beads, amplified, and sequenced on a HiSeq 2500 platform (Illumina). Sequencing of SureSelect DNA libraries (paired-end 2 × 101-bp reads) generated approximately 120 000 000 (102 048 924-131 440 392) reads for each sample.

2.4 | Mapping and single nucleotide variant/insertion and deletion calling

Adapter and low-quality sequences were removed by Cutadapt (v. 1.2.1).[9] Contaminated reads derived from mouse tissues were removed by DeconSeq (v. 0.4.3)[10] using mouse genome (genome assembly release name: mm10). Reads were mapped to the reference genome (Human GRCh37/hg19), using BWA-MEM (v. 0.7.10)[11] with default parameters. Duplicated reads were removed by Picard (v. 1.73), and local realignment and base quality recalibration were carried out by GATK (v. 1.6-13).[12] Single nucleotide variant (SNV) and insertion and deletion (indel) calls were carried out with multi-sample calling using the GATK UnifiedGenotyper and filtered to coordinates with VQSR passed and variant call quality score ≥30. Annotations of SNV and indels were based on dbSNP149, CCDS (NCBI, Release 15), RefSeq (UCSC Genome Browser, Feb 2017), Gencode (UCSC Genome Browser, ver. 19), and 1000Genomes (phase 3 release v5). Predicted functions of variants were further filtered according to the following criteria: frameshift, nonsense, read-through, missense, deletion, insertion, or insertion-deletion.

2.5 | Library preparation and sequencing for transcriptome analysis

Total RNA of PDX and SRT was extracted using Nucleo Spin RNA kits (Takara Bio). Each total RNA sample (0.5 μg), extracted from six paired samples of PDX and SRT, was converted into a RNA-seq library of template molecules suitable for subsequent cluster generation using the Illumina TruSeq RNA Sample Preparation Kit v. 2 (Illumina) according to the manufacturer's protocol. The first step was purifying the poly-A-containing mRNA molecules using poly-T oligo-attached magnetic beads. Following purification, the mRNA

was fragmented into small pieces using divalent cations at elevated temperature. The cleaved RNA fragments were copied into first-strand cDNA using reverse transcriptase and random primers. This was followed by second-strand cDNA synthesis using DNA polymerase I and RNase H. These cDNA fragments then go through an end repair process, the addition of a single 'A' base, and then ligation of the adapters. Next, the products are purified and enriched with PCR to create the final cDNA library. The result of the fragmentation step is an RNA-seq library that includes inserts that range in peak size from 368 bp to 405 bp. The libraries were sequenced on a HiSeq 2500 platform (Illumina). Sequencing of TruSeq RNA libraries (paired-end 2 × 101 bp reads) generated approximately 50 000 000 (47 467 804-56 123 818) reads for each sample. Raw sequencing data are available from the Gene Expression Omnibus (https://www.ncbi.nlm.nih.gov/geo/query/acc.cgi?acc=GSE130160) under the accession number GSE130160.

2.6 | Transcriptome analysis

Adapter and low-quality sequences were removed by Cutadapt (v. 1.2.1).[9] After quality control, poly-A/T sequences were also removed by PRINSEQ (v. 0.19.2).[13] The trimmed reads were mapped to the reference human genome (GRCh37/hg19) using TopHat (v. 2.0.13).[14] Mapped reads were assembled by Cufflinks (v. 2.2.1),[15] and the transcripts across all samples were merged by Cuffmerge. Fragments per kilo base per million map reads (FPKM) was calculated with Cuffquant. Cuffquant and Cuffdiff are programs involved in the Cufflinks package.

2.7 | Correlation and clustering analysis for somatic mutations

Spearman's rank correlation analysis was conducted for converted numeral data based on numbers of minor alleles in each detected non-synonymous mutation and correlation coefficients were calculated in all 12 samples. Six PDX SRT pairs were more highly correlated ($\rho > .9$) than the remaining pairs ($\rho < .5$). Hierarchical clustering based on Spearman's rank correlation coefficient and average-linkage was conducted for converted numeral data to confirm similarity in somatic mutations of six pairs of PDX and SRT using R library, pvclust.[16]

Approximately unbiased (AU) *P*-value and bootstrap probability (BP) *P*-value were calculated using default settings (n = 1000) with pvclust. The six-pairs of PDX and SRT were clustered with 100 AU and 100 BP values.

2.8 | Visualization based on heatmap for gene expression and copy number

Gene expression based on FPKM were log-transformed and normalized using all genes. The heatmap images of normalized gene expression and gene-level copy numbers were illustrated using the heatmap.2 function in R library, gplots[17] for 301 cancer-related genes.

2.9 | Treatment of PDX with EGFR-TKI

Tumor fragments from adenocarcinomas with *EGFR*-activating mutations (#7, #11) were implanted into SHO mice. When tumor volume exceeded 500 mm^3, the mice were treated by oral gavage with 25 mg/kg per day osimertinib, 25 mg/kg per day gefitinib, and 25 mg/kg per day crizotinib. Mice were killed when tumor volume reached 1500 mm^3.

2.10 | Immunoblot analyses

Patient-derived xenograft tumor lysates were prepared using cell lysis buffer (Cell Signaling) and immunoblotting was carried out as previously described.[18] All antibodies were purchased from commercial companies as follows: anti-E-cadherin, anti-Vimentin, anti-ZEB1, anti-β-actin (13E5) (Cell Signaling Technology), diluted at a ratio of 1:1000. Antigen-antibody reaction bands were visualized with the SuperSignal West Dura Extended Duration Substrate, an ECL substrate (Pierce Biotechnology). Experiments were independently repeated at least three times.

3 | RESULTS

3.1 | Establishment of PDX from surgically resected NSCLC tumors

Characteristics of 30 NSCLC patients are shown in Table 1 and Table S1. In the first 14 cases, PDX with stable growth were developed: 3/12 (25%) in SHO mice and 2/7 (29%) in NOD mice. In the next 16 cases, we implanted SRT in SHO mice only. In total, 10 stable PDX lines were established, which could be serially passaged. Rate of established PDX was 33.3% (10/30), 16.7% (3/18) in AD, 60% (6/10) in SQ, and 50% (1/2) in LA. Eight out of 18 AD (44.4%) had *EGFR* mutations (L858R or exon 19 deletion) and, of these, two generated PDX with stable growth. The *ALK* fusion gene was detected in one PDX but it failed to establish stable growth.

We compared the characteristics of patients whose tumors developed stably growing PDX with patients whose tumors failed to do so. Histology of SQ, advanced clinical stage (III-IV), status of lymph node metastasis (N2-3), and standardized uptake value (SUV) max at delayed scan in FDG-PET (≥10), but not age, gender, smoking history, status of primary tumor (T factor) or metastasis (M factor), were associated with development of stably growing PDX (Table 2).

3.2 | Histological comparison of PDX and SRT

Next, we compared morphology using H&E staining in 10 pairs of mice SRT and their corresponding PDX after two to six passages. PDX generally maintained the morphological characteristics of corresponding SRT (Figure 1 and Figure S1), although tumors of PDX #7, #8, and #11 showed slightly poorer differentiated features compared with the corresponding SRT.

TABLE 1 Characteristics of patients whose tumors established PDX

Case	Age (y)	Gender	Smoker (pack years)	Tumor type	TNM	Stage	SUV max (delay)	Driver oncogene
#2	75	Male	82.5	Squamous	2a20	III A	13.1	WT
#5	70	Male	84.0	Squamous	2a00	I B	23	WT
#7	81	Male	56.0	Adeno	2a20	III A	34.1	EGFR exon 21 L858R
#8	69	Male	72.0	Adeno	2b00	II A	ND	NE
#10	73	Male	84.0	Squamous	2a20	III A	11.6	WT
#11	69	Male	10.0	Adeno	2a11a	IV	12.4	EGFR exon 19 del
#16	72	Male	52.0	Squamous	1b20	III A	16.2	WT
#21	72	Male	60.0	Squamous	1c00	I A3	11.5	NE
#22	60	Male	30.0	Squamous	2b10	II B	16.5	WT
#30	51	Male	26.3	Large	2a00	I B	20.1	WT

Adeno, adenocarcinoma; del, deletion; EGFR, epidermal growth factor receptor; Large, large cell carcinoma; ND, not detected; NE, not evaluated; PDX, patient-derived xenograft; Squamous, squamous cell carcinoma; SUV, standardized uptake value; WT, wild type.

Of the 10 PDXs, we chose the six that were first to establish (cases #2, #5, #7, #10, #11, and #16) and compared profiles of protein expression, DNA mutations, and mRNA expression to corresponding SRT. IHC showed that expression of human PD-L1 and MHC-class I was heterogeneous among six SRT and could be changed in corresponding PDX (Table 3). Percentage of PD-L1-positive tumor cells

TABLE 2 Correlation between clinical characteristics and establishment of PDX

Parameters	Class	Establishment rate (%)	P-value*
Gender	Male	10/24 (41.7)	.065
	Female	0/6 (0)	
Age (y)	<70	4/12 (33.3)	.31
	≥70	6/18 (33.3)	
Smoker pack years	<10	0/6 (0)	.065
	≥10	10/24 (41.7)	
Tumor type	Adeno	3/18 (16.7)	.025**
	Squamous	6/10 (60.0)	
T	<T2b	8/22 (36.4)	.30
	≥T2b	2/8 (25.0)	
N	<N1	4/21 (19.0)	.008**
	≥N1	6/8 (75.0)	
M	M0	9/28 (32.1)	.46
	M1	1/2 (50.0)	
Stage	<3A	5/23 (21.7)	.024**
	≥3A	5/7 (71.4)	
SUV max (delay)	<10	0/8 (0)	.024**
	≥10	9/20 (45)	

SUV, standardized uptake value.

*P-values were calculated by the Fisher's exact test.

**P < .05.

was increased in PDX #2, #7, #10, and #11; decreased in PDX #16; and unchanged in PDX #5, compared with the corresponding SRT. Percentage of MHC-class I-positive tumor cells was increased in PDX #7, #11, and #16; decreased in PDX #5 and #10; and unchanged in PDX #2, compared with the corresponding SRT.

Human cell markers CD8, CD68, MPO, and CD31 were positive in all SRT. In PDX, they were negative, and murine CD31 and F4/80 were positive after two to six passages. These findings clearly indicate that stroma of PDX can be replaced by murine cells after several passages.

3.3 | Whole-exome sequencing of SRT and PDX

We carried out whole-exome sequencing of the six pairs of PDX and SRT. More than 13 000 non-synonymous mutations were detected in all PDX and SRT (Table S2). The six pairs preserved 80%-90% of the non-synonymous mutations between PDX and SRT (Figure 2A). Analysis of 20 cancer-associated genes showed that mutations in those genes, including EGFR-L858R in case #7 and EGFR-exon 19 deletion in case #11, were generally preserved between PDX and SRT (Figure 2B). Correlation and clustering analysis of somatic mutation showed that each pair of PDX and SRT formed a rigid cluster (Figure 2C,D), indicating the similarity of somatic mutations in PDX and their corresponding SRT. We estimated copy number alterations (CNA) (Appendix S1). SRT #7 showed high copy numbers of EGFR, which had the L858R mutation, and the EGFR copy number was substantially increased in its corresponding PDX (Figure S2).

3.4 | Transcriptome analysis of PDX and SRT

We next explored mRNA expression in 201 cancer-associated genes. Several signal transduction-related genes, including AKT1, CTNNB1, JUN, MAPK1, and YES1; receptor tyrosine kinases, including EGFR

FIGURE 1 Histological appearance of surgically resected tumors (SRT) and patient-derived xenografts (PDX). Morphology of H&E-stained SRT and PDX sections was compared in 10 pairs of SRT and their corresponding PDX after two to six passages. Three AC (cases #7, #8, #11), six SC (cases #2, #5, #10, #16, #21, #22), and one LC (case #30) are shown. Scale bar, 100 μm
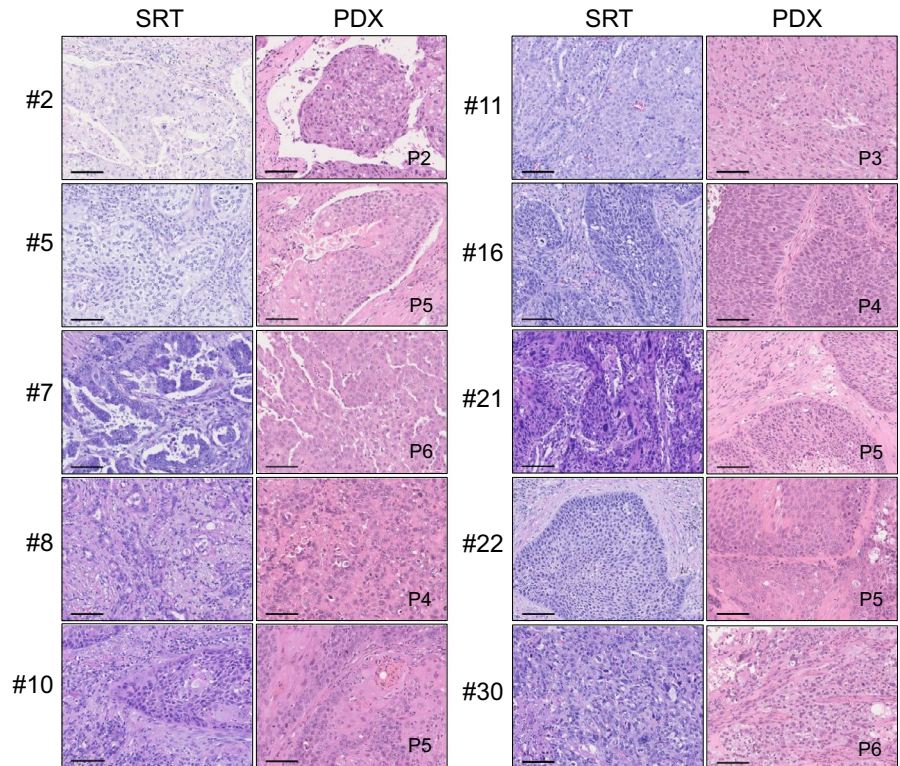

TABLE 3 Expression of human and murine markers in PDX and SRT

			Anti-human Ab							Anti-murine Ab	
			Tumor cells		Stroma cells					Stroma cells	
Histology		Tumor	PD-L1 (22C3)	MHC Class I	CD8 (Ly)	CD68 (Mo)	MPO (Neu)	CD31 (EC)	SMA (Fib)	CD31 (EC)	F4 80 (Mo)
#2	SQ	SRT	30%	100%	2+	2+	1+	2+	2+	—	—
		PDX	80%	100%	0	0	0	0	2+	2+	1+
#5	SQ	SRT	90%	20%	1+	1+	2+	2+	2+	—	—
		PDX	90%	0%	0	0	0	0	2+	2+	1+
#7	AD	SRT	70%	70%	2+	1+	1+	1+	2+	—	—
		PDX	90%	100%	0	0	0	0	2+	1+	2+
#10	SQ	SRT	30%	70%	1+	1+	1+	2+	2+	—	—
		PDX	70%	50%	0	0	0	0	2+	2+	1+
#11	AD	SRT	20%	80%	1+	1+	1+	2+	2+	—	—
		PDX	60%	100%	0	0	0	0	1+	1+	2+
#16	SQ	SRT	10%	10%	1+	1+	1+	2+	2+	—	—
		PDX	0%	100%	0	0	0	0		1+	1+

22C3, 22C3 clone; AD, adenocarcinoma; EC, endothelial cells; Fib, fibroblast; Ly, lymphocytes; Mo, monocytes; MPO, myeloperoxidase; Neu, neutrophil; PD-L1, programmed cell death 1 ligand; PDX, patient-derived xenograft; SMA, smooth muscle actin; SQ, squamous cell carcinoma; SRT, surgically resected tumor.

and DDR1; and angiogenesis-related genes, including vascular endothelial growth factor A (VEGFA) and transforming growth factor beta 1 (TGFB1), were highly expressed in all PDX and SRT (Figure 3). In contrast, angiogenesis-related genes, mainly expressed in pericytes and endothelial cells (such as platelet derived growth factor receptor beta 1 [PDGFRB1] and VEGFR2) and chemokines, mainly expressed in leukocytes (such as chemokine [C-C motif] ligand 5 [CCL5] and C-X-C motif chemokine ligand 9 [CXCL9]), were highly expressed in SRT but not in PDX. This is consistent with the results of IHC which indicated the replacement of host cells with mouse cell components in PDX. These results indicate that mRNA expression of several cancer-associated genes could be preserved in PDX.
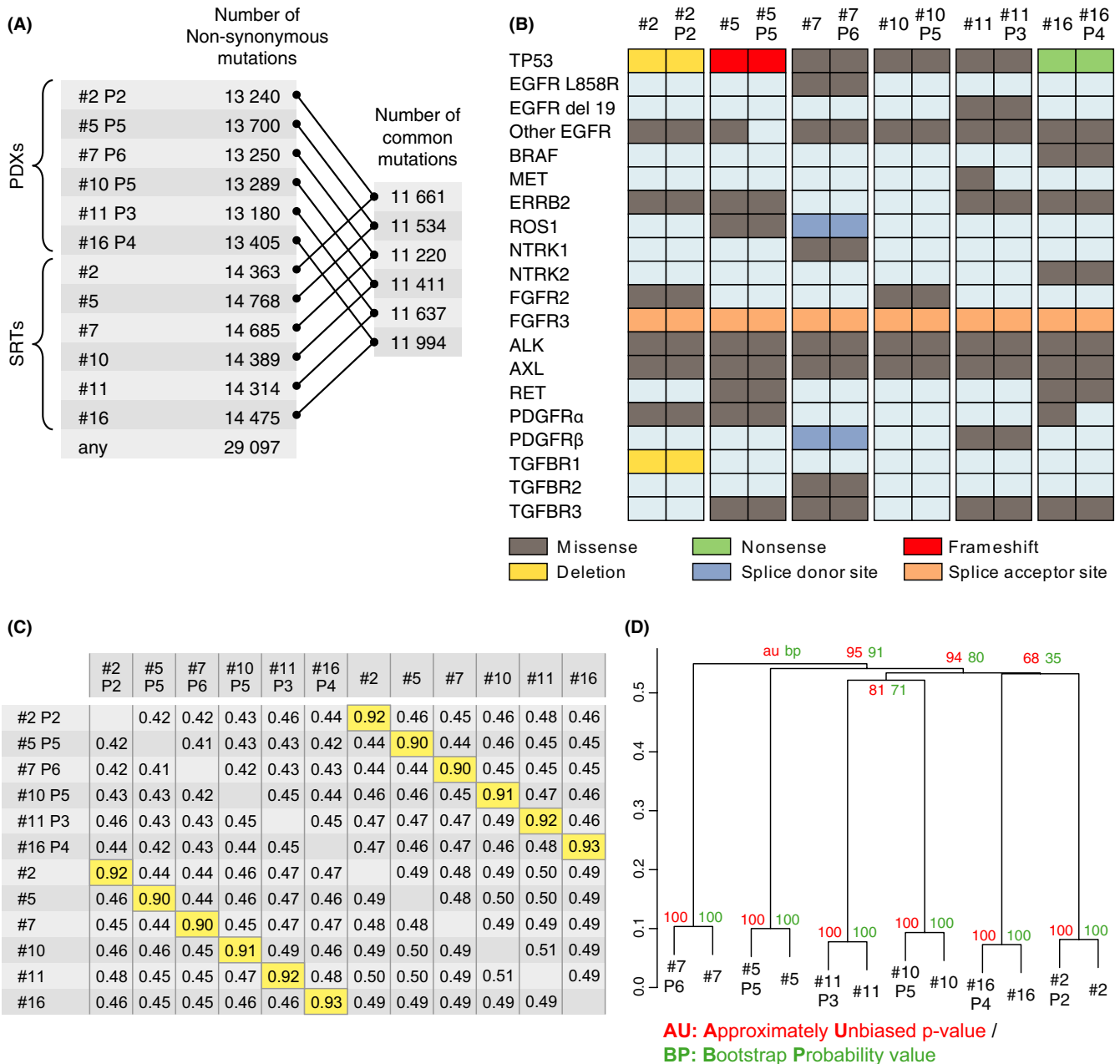
FIGURE 2 Comparison of somatic mutations in patient-derived xenografts (PDX) and surgically resected tumors (SRT). Six PDX paired with their corresponding SRT were used for whole-exome sequencing. A, Approximately 13 000 non-synonymous mutations were detected. B, Twenty cancer-associated gene mutations were compared between PDX and SRT. C and D, PDX and SRT were analyzed by correlation (C) and clustering analysis (D)

In RNA sequencing, we detected 161 fusion-genes by STAR-Fusion analyses and 350 by deFuse analyses (Appendix S1, Tables S3 and S4). Putative driving gene fusion was detected in LAMA5-LAMP3 in pair #10. This was the only in-frame and inter-chromosomal fusion gene, detected by STAR-Fusion and deFuse analyses.

3.5 | Susceptibility of PDX to targeted drugs

We explored the susceptibility of two PDX (#7 and #11) with *EGFR* mutations to EGFR-TKI osimertinib, which is recognized as the standard first-line treatment for advanced *EGFR* mutated NSCLC.[19] Osimertinib rapidly decreased the size of PDX case #7 during the

FIGURE 3 Heat map of expression of 201 cancer-associated genes in patient-derived xenografts (PDX) and surgically resected tumors (SRT). Six PDX paired with their corresponding SRT were used for mRNA expression analysis of 201 cancer-associated genes, including signal transduction-related genes, receptor tyrosine kinases, and angiogenesis-related genes
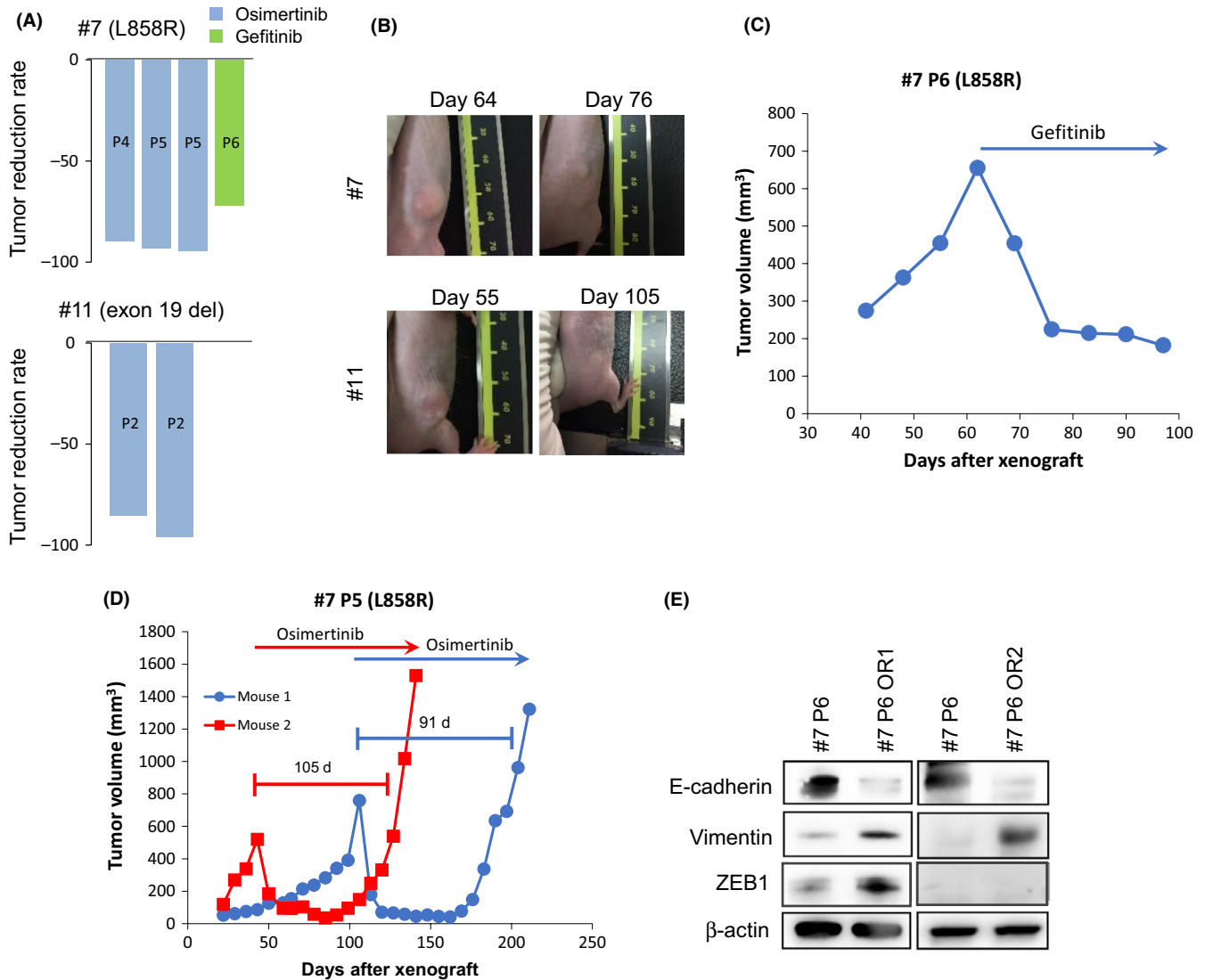
Color Key

Z value of Log10(FPKM)
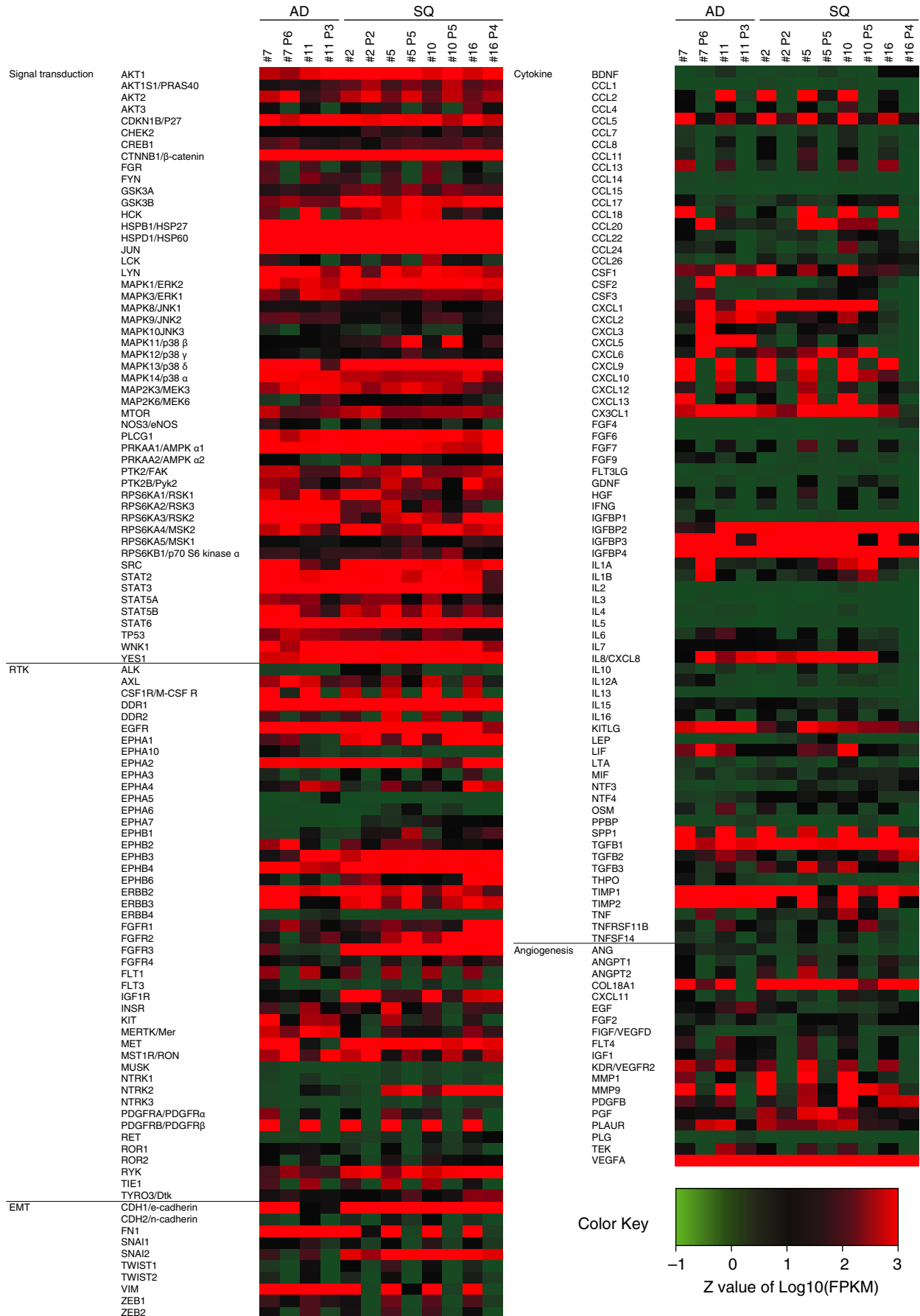
FIGURE 4 Susceptibility of epidermal growth factor receptor (*EGFR*) activating mutation-positive patient-derived xenografts (PDX) to EGFR-TKI in vivo. Mice inoculated with *EGFR* mutation-positive PDX (#7 and #11) were treated by EGFR-TKI. A, Rate of tumor shrinkage is shown by waterfall plot. B, Photos taken before and after osimertinib treatment (25 mg/kg per day) are shown. C, Timeline of tumor volume in PDX #7 treated with gefitinib (25 mg/kg per day). D, Induction of resistance by continuous osimertinib treatment (25 mg/kg per day, N = 2). E, Epithelial-mesenchymal transition markers were assessed by immunoblots. TKI, tyrosine kinase inhibitors

fourth to fifth passage and of PDX case #11 after the second passage (Figure 4A,B). As case #7 recurred after surgery and as gefitinib treatment resulted in remarkable tumor regression in this patient, we also examined the effect of gefitinib against PDX #7. Gefitinib caused a rapid decrease in the size of PDX #7 (Figure 4C), consistent with its efficacy in the patient. These results indicate that even after repeated passages PDX remained sensitive to targeted drugs. Moreover, these results suggest high sensitivity to osimertinib in these two patients.

We further assessed whether osimertinib resistance could be induced in PDX models by continuous oral treatment with osimertinib. Although the PDX tumor in case #11 was cured by osimertinib treatment, the PDX tumor in case #7 regrew during the continuous osimertinib treatment (Figure 4D). We detected the activating mutation in *EGFR* (mutation L858R), but no known resistance mutations

such as T790M or C797S.[20,21] Phosphorylation of receptor tyrosine kinases, including MET, HER2, HER3, or AXL, was not remarkably increased (data not shown). Immunoblots showed that expression of mesenchymal marker vimentin increased, whereas expression of epithelial marker E-cadherin decreased in the resistant tumor when compared with the parental tumor (Figure 4E). These results strongly suggest that this PDX acquired the mesenchymal phenotype and therefore became resistant to osimertinib.

As we could obtain organoid culture from PDX #7 P6 OR1, we carried out cell viability assay with inhibitor of bypass pathways. We treated the organoids with AXL inhibitor (NPS-1034), which also has activity to MET inhibition (IC$_{50}$ for AXL and MET are 10.3 and 48 nmol/L, respectively) at 1 μmol/L in the presence or absence of osimertinib (1 μmol/L). Osimertinib at 1 μmol/L decreased the viability of organoid by 20% but NPS-1034 did not remarkably affect

the viability, irrespective of the presence of osimertinib. These data suggest that AXL was not involved in osimertinib resistance in #7 P6 OR1 organoids (Figure S3). We recently reported that inhibition of histone deacetylase (HDAC) is a therapeutic candidate to overcome EMT-mediated ALK inhibitor resistance.[22] We therefore further examined the effect of HDAC inhibition on sensitivity to EGFR inhibitors using organoid culture #7 P6 OR1. Very interestingly, either osimertinib or HDAC inhibitor quisinostat inhibited viability of the organoids by 50%, and pretreatment of quisinostat followed by osimertinib further suppressed the viability (Figure S4). These data suggest that HDAC inhibition may overcome EMT-associated resistance not only to ALK-TKI, but also to EGFR-TKI.

4 | DISCUSSION

In the present study, we established 10 PDX mainly in SHO mice using SRT from 30 NSCLC patients. Interestingly, SQ developed PDX more frequently than AD. We have no clear answer to this result, but higher PDX-establishment rate of SQ compared with AD was reported in many studies.[23-25] SQ is known to occur by multistep carcinogenesis,[26,27] and colon cancer, which is also known to occur by multistep carcinogenesis, develops PDX at a high incidence. In contrast, tumors with driver oncogenes such as EGFR mutations and EML4-ALK developed at a much lower incidence.[28,29] Therefore, tumors occurring by multistep carcinogenesis might tend to develop PDX. Moreover, tumors obtained from patients whose SUVmax ≥10 from a delayed FDG-PET scan developed PDX more frequently than those of patients with SUVmax <10. The reason why a high SUVmax value in the delayed scan, but not in the early scan, correlated with higher PDX establishment success rates is unclear at present. This study used a relatively small sample size, and further evaluation with larger numbers of patients is warranted.

Recent studies reported that PDX models have various advantages over CDX models, including maintaining the histological appearance of the original tumor, tumor cell heterogeneity in a single lesion, and inclusion of critical stromal elements.[30] We confirmed that histological appearance was generally preserved in PDX. However, stromal components were completely replaced by murine cells after several passages, suggesting limited use for PDX in analyzing tumor-host interactions and immune responses. However, PDX preserved somatic mutations and mRNA expression of the corresponding SRT. These results support the use of PDX for evaluation of characteristics and drug sensitivity in vivo. Clinical response to gefitinib in case #7 corresponded with gefitinib sensitivity in the PDX which preserved the EGFR-L858R mutation. In addition, PDX from cases #7 and #11, both of which had EGFR-activating mutations, were highly sensitive to osimertinib which is the standard targeted drug for EGFR-mutated NSCLC. The high sensitivity of these PDX to osimertinib was not substantially changed even after several passages. This suggests that PDX are suitable models for the prediction of clinical responses to targeted drugs in the corresponding patients, as well as a screening tool for the efficacy of novel drugs.

Acquired resistance is the critical problem impacting targeted drug therapies. We induced acquired resistance to osimertinib in one of two PDX with different EGFR mutations. Osimertinib cured PDX with EGFR-exon 19 deletion, which is known to be more sensitive to EGFR-TKI, compared with the EGFR-L858R mutation.[31] In addition, transcriptome analysis showed that PDX #7 expressed higher levels of AXL than PDX #11. We recently reported that AXL promotes the emergence of cells tolerant to osimertinib.[32] Therefore, AXL may facilitate the emergence of osimertinib-tolerant tumor cells and advance to the acquired resistance seen in PDX #7. Very interestingly, two PDX tumors passaged from a PDX with EGFR-L858R acquired osimertinib resistance after very similar progression-free periods (13-15 weeks). Both of the resistant PDX showed EMT but no known resistance mutations in EGFR. These results indicate that PDX may be reproducible models in terms of treatment periods for resistance induction and mechanisms of resistance when using tumors with the same origin. EMT is associated with resistance to various targeted drugs including EGFR-TKI and ALK-TKI[33] and is sometimes detected simultaneously with resistance mutations in a single resistant lesion.[34] We have reported that EMT is a mechanism of ALK-TKI resistance independent of ALK resistance mutation status.[22] In the present study, E-cadherin expression was decreased in both #7 P6 OR1 and #7 P6 OR2, compared with #7. Interestingly, ZEB1 expression was increased in #7 P6 OR1, but not #7 P6 OR2, whereas vimentin expression was increased in both #7 P6 OR1 and #7 P6 OR2, compared with #7. ZEB1 expression is not always increased in mesenchymal cells as suggested in the literature.[35] Collectively, we concluded that both #7 P6 OR1 and #7 OR2 have mesenchymal phenotype rather than epithelial phenotype (Figure S5). Our PDX model with osimertinib resistance may be useful to clarify the precise resistance mechanisms and develop novel therapies to overcome resistance as a result of EMT.

In summary, we established 10 serially transplantable PDX of NSCLC in SHO mice and showed the utility of the PDX with an EGFR mutation for analyses of EGFR-TKI resistance. Further study is needed to clarify the mechanism of EMT-associated EGFR-TKI resistance and establish efficient therapy to overcome this resistance.

DISCLOSURE

Seiji Yano has received honorarium from Chugai. The other authors have no conflicts of interest to declare.

ORCID

Kenji Kita https://orcid.org/0000-0002-4622-6633

Hiro Takahashi https://orcid.org/0000-0002-8230-9524

Seiji Yano https://orcid.org/0000-0002-6151-2988

REFERENCES

1. Boven E, Winograd B, Berger DP, et al. Phase II preclinical drug screening in human tumor xenografts: a first European multicenter collaborative study. *Cancer Res*. 1992;52(21):5940-5947.
2. Marangoni E, Vincent-Salomon A, Auger N, et al. A new model of patient tumor-derived breast cancer xenografts for preclinical assays. *Clin Cancer Res*. 2007;13(13):3989-3998.
3. Fichtner I, Rolff J, Soong R, et al. Establishment of patient-derived non-small cell lung cancer xenografts as models for the identification of predictive biomarkers. *Clin Cancer Res*. 2008;14(20):6456-6468.
4. Hidalgo M, Amant F, Biankin AV, et al. Patient-derived xenograft models: an emerging platform for translational cancer research. *Cancer Discov*. 2014;4(9):998-1013.
5. Gao H, Korn JM, Ferretti S, et al. High-throughput screening using patient-derived tumor xenografts to predict clinical trial drug response. *Nat Med*. 2015;21(11):1318-1325.
6. Drapkin BJ, George J, Christensen CL, et al. Genomic and functional fidelity of small cell lung cancer patient-derived xenografts. *Cancer Discov*. 2018;8(5):600-615.
7. Maekawa H, Miyoshi H, Yamaura T, et al. A chemosensitivity study of colorectal cancer using xenografts of patient-derived tumor-initiating cells. *Mol Cancer Ther*. 2018;17(10):2187-2196.
8. Choi YY, Lee JE, Kim H, et al. Establishment and characterisation of patient-derived xenografts as paraclinical models for gastric cancer. *Sci Rep*. 2016;6:22172.
9. Martin M. Cutadapt removes adapter sequences from high-throughput sequencing reads. *EMBnet J*. 2011;17:10-12.
10. Schmieder R, Edwards R. Fast identification and removal of sequence contamination from genomic and metagenomic datasets. *PLoS ONE*. 2011;6(3):e17288.
11. Li H, Durbin R. Fast and accurate short read alignment with Burrows-Wheeler transform. *Bioinformatics*. 2009;25:1754-1760.
12. McKenna A, Hanna M, Banks E, et al. The genome analysis toolkit: a MapReduce framework for analyzing next-generation DNA sequencing data. *Genome Res*. 2010;20(9):1297-1303.
13. Schmieder R, Edwards R. Quality control and preprocessing of metagenomic datasets. *Bioinformatics*. 2011;27(6):863-864.
14. Kim D, Pertea G, Trapnell C, et al. TopHat2: accurate alignment of transcriptomes in the presence of insertions, deletions and gene fusions. *Genome Biol*. 2013;14:R36.
15. Trapnell C, Williams BA, Pertea G, et al. Transcript assembly and quantification by RNA-Seq reveals unannotated transcripts and isoform switching during cell differentiation. *Nat Biotechnol*. 2010;28(5):511-515.
16. Suzuki R, Shimodaira H. Pvclust: an R package for assessing the uncertainty in hierarchical clustering. *Bioinformatics*. 2006;22(12):1540-1542.
17. Warnes GR, Bolker B, Bonebakker L, et al. gplots: Various R programming tools for plotting data, R package version 2 (4), 1; 2009.
18. Arai S, Kita K, Tanimoto A, et al. *In vitro* and *in vivo* anti-tumor activity of alectinib in tumor cells with NCOA4-RET. *Oncotarget*. 2017;8(43):73766-73773.
19. Soria JC, Ohe Y, Vansteenkiste J, et al. Osimertinib in untreated EGFR-mutated advanced non-small-cell lung cancer. *N Engl J Med*. 2018;378(2):113-125.
20. Pao W, Miller VA, Politi KA, et al. Acquired resistance of lung adenocarcinomas to gefitinib or erlotinib is associated with a second mutation in the EGFR kinase domain. *PLoS Med*. 2005;2(3):e73.
21. Ercan D, Choi HG, Yun CH, et al. EGFR mutations and resistance to irreversible pyrimidine-based EGFR inhibitors. *Clin Cancer Res*. 2015;21(17):3913-3923.
22. Fukuda K, Takeuchi S, Arai S, et al. Epithelial-to-mesenchymal transition is a mechanism of ALK inhibitor resistance in lung cancer independent of ALK mutation status. *Cancer Res*. 2019;79(7):1658-1670.
23. Julien S, Merino-Trigo A, Lacroix L, et al. Characterization of a large panel of patient-derived tumor xenografts representing the clinical heterogeneity of human colorectal cancer. *Clin Cancer Res*. 2012;18(19):5314-5328.
24. John T, Kohler D, Pintilie M, et al. The ability to form primary tumor xenografts is predictive of increased risk of disease recurrence in early-stage non-small cell lung cancer. *Clin Cancer Res*. 2011;17:134-141.
25. Fang T, Huang H, Li X, et al. Effects of siRNA silencing of TUG1 and LCAL6 long non-coding RNAs on patient-derived xenograft of non-small cell lung cancer. *Anticancer Res*. 2018;38(1):179-186.
26. Lee HW, Lee JI, Lee SJ, et al. Patient-derived xenografts from non-small cell lung cancer brain metastases are valuable translational platforms for the development of personalized targeted therapy. *Clin Cancer Res*. 2015;21(5):1172-1182.
27. Bennett WP, Colby TV, Travis WD, et al. p53 protein accumulates frequently in early bronchial neoplasia. *Cancer Res*. 1993;53(20):4817-4822.
28. Hirano T, Franzén B, Kato H, et al. Genesis of squamous cell lung carcinoma. Sequential changes of proliferation, DNA ploidy, and p53 expression. *Am J Pathol*. 1994;144(2):296-302.
29. Kosaka T, Yatabe Y, Endoh H, et al. Mutations of the epidermal growth factor receptor gene in lung cancer: biological and clinical implications. *Cancer Res*. 2004;64(24):8919-8923.
30. Soda M, Choi YL, Enomoto M, et al. Identification of the transforming EML4-ALK fusion gene in non-small-cell lung cancer. *Nature*. 2007;448(7153):561-566.
31. Jackman DM, Yeap BY, Sequist LV, et al. Exon 19 deletion mutations of epidermal growth factor receptor are associated with prolonged survival in non-small cell lung cancer patients treated with gefitinib or erlotinib. *Clin Cancer Res*. 2006;12(13):3908-3914.
32. Taniguchi H, Yamada T, Wang R, et al. AXL confers intrinsic resistance to osimertinib and advances the emergence of tolerant cells. *Nat Commun*. 2019;10(1):259.
33. Nieto MA, Huang RY, Jackson RA, et al. EMT: 2016. *Cell*. 2016;166(1):21-45.
34. Gainor JF, Dardaei L, Yoda S, et al. Molecular mechanisms of resistance to first- and second-generation ALK inhibitors in ALK-rearranged lung cancer. *Cancer Discov*. 2016;6:1118-1133.
35. Jägle S, Dertmann A, Schrempp M. ZEB1 is neither sufficient nor required for epithelial-mesenchymal transition in LS174T colorectal cancer cells. *Biochem Biophys Res Commun*. 2017;482(4):1226-1232.

SUPPORTING INFORMATION

Additional supporting information may be found online in the Supporting Information section at the end of the article.